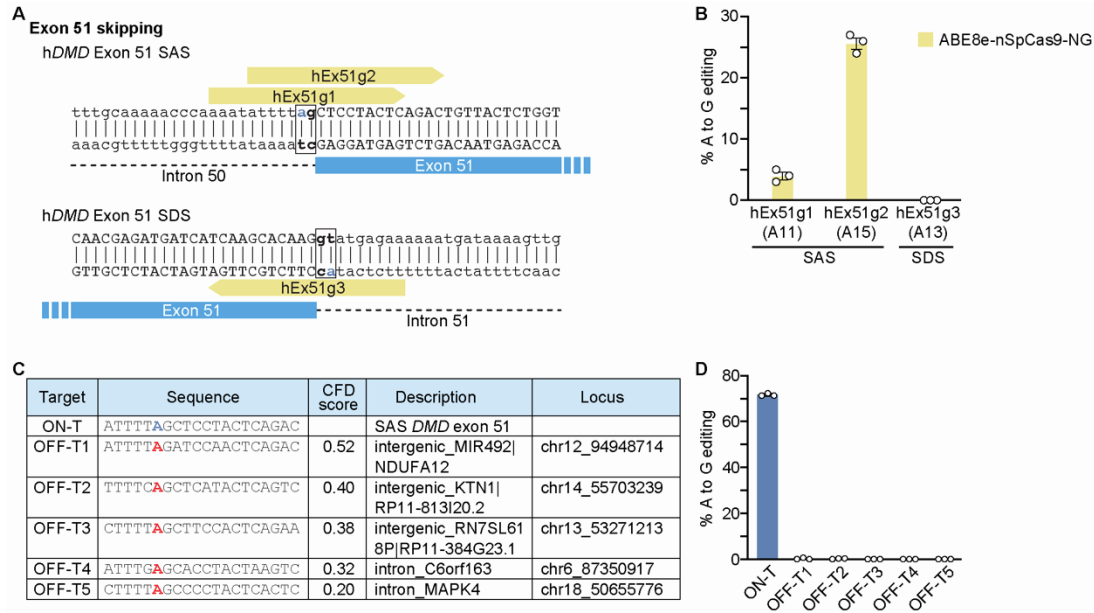


**OMTN, Volume 32**

**Supplemental information**

**Single-swap editing for the correction  
of common Duchenne muscular  
dystrophy mutations**

**Andreas C. Chai, Francesco Chemello, Hui Li, Takahiko Nishiyama, Kenian Chen, Yu Zhang, Efraín Sánchez-Ortiz, Adeeb Alomar, Lin Xu, Ning Liu, Rhonda Bassel-Duby, and Eric N. Olson**



**Figure S1. Identification of the most efficient ‘single-swap’ guide for exon skipping of *DMD* Exon 51.** (A) Schematic of candidate sgRNAs for single-swap editing at the SAS or SDS of *DMD* exon 51. Target adenines in relation to candidate sgRNAs are indicated in blue. Canonical splice site motifs are in bold and boxed. (B) Editing efficiency by Sanger sequencing of target adenine using candidate sgRNAs with ABE8e-nSpCas9-NG following transient transfection in HEK293T cells. The editing efficiency of the most efficient guide, hEx51g2, is  $25.7 \pm 1.7\%$  (C) Candidate off-target sites within the human genome for hEx51g2 as identified by CRISPOR and ranked by Cutting Frequency Determination (CFD) score. Target adenine of *DMD* exon 51 SAS is highlighted in blue. Corresponding adenines at off-target sites are highlighted in red. (D) Editing efficiency by Sanger sequencing of target adenines at on-target ( $71.6 \pm 0.6\%$ ) and potential off-target sites ( $<0.2\%$ ) in  $\Delta$ Ex48-50 iPSCs. Data are mean  $\pm$  s.d.  $n = 3$  independent replicates.

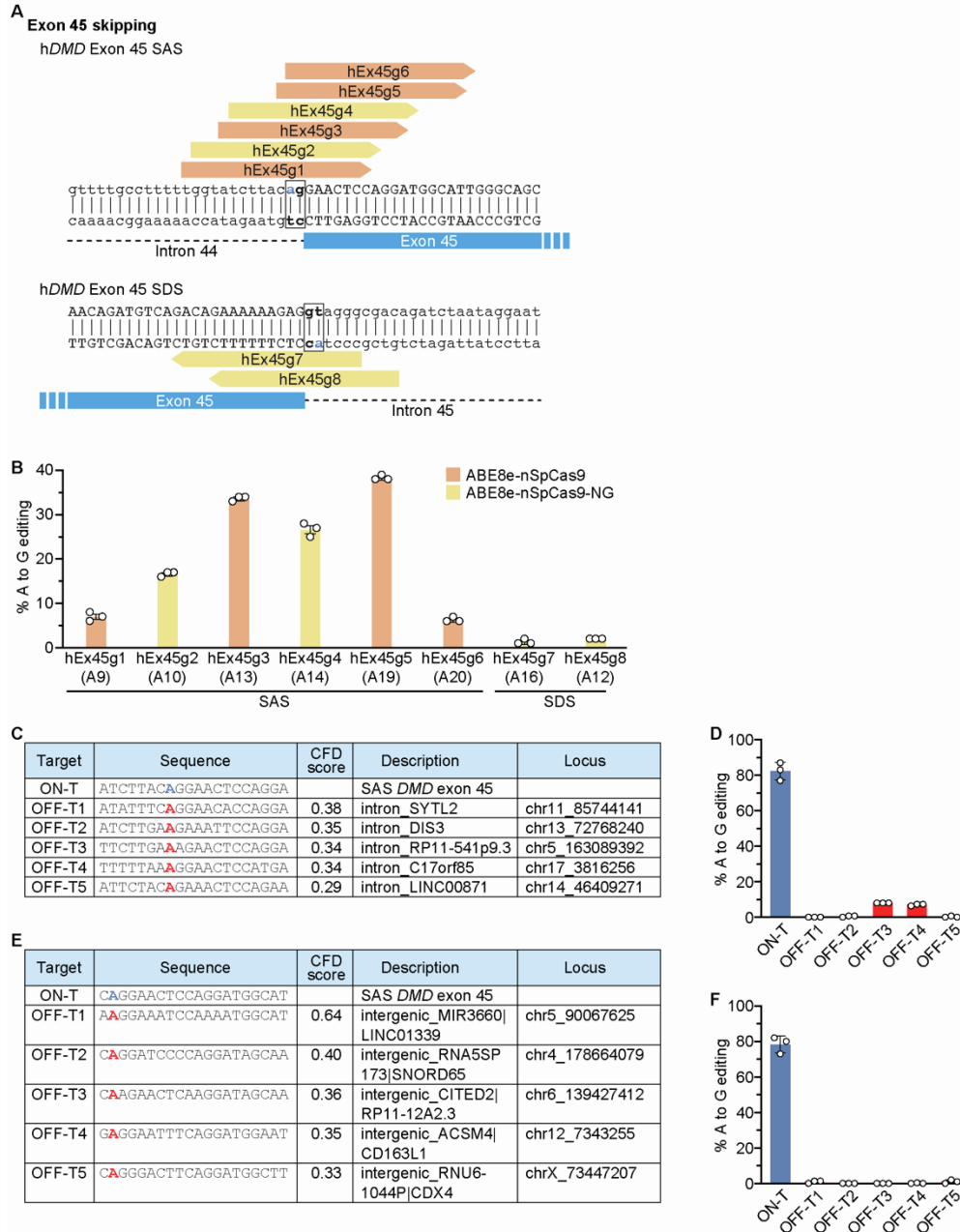


**Figure S2. Identification of the most efficient ‘single-swap’ guide for exon skipping of *DMD***

**exon 45. (A)** Schematic of candidate sgRNAs for single-swap editing at the SAS or SDS of

*DMD* exon 45. Target adenines in relation to candidate sgRNAs are indicated in blue. Canonical

splice site motifs are in bold. **(B)** Editing efficiency by Sanger sequencing of target adenine using

candidate sgRNAs with ABE8e-nSpCas9-NG or ABE8e-nSpCas9 following transient

transfection in HEK293T cells. The editing efficiencies of the most efficient guides, hEx45g3

and hEx45g5, are  $33.7 \pm 0.6\%$  and  $38.3 \pm 0.6\%$ , respectively. **(C)** Candidate off-target sites within the human genome for hEx45g3 as identified by CRISPOR and ranked by CFD score. Target adenine of exon 45 SAS is highlighted in blue. Corresponding adenines at off-target sites are highlighted in red. **(D)** Editing efficiency of target adenines at on-target ( $83.3 \pm 5.0\%$ ) and potential off-target sites for hEx45g3 in  $\Delta$ Ex44 iPSCs. Significant editing was found at OFF-T3 ( $8.0 \pm 0.0\%$ ) and OFF-T4 ( $7.0 \pm 0.6\%$ ) sites.  $n = 3$  independent replicates. **(E)** Candidate off-target sites within the human genome for hEx45g5 as identified by CRISPOR and ranked by CFD score. Target adenine of exon 45 SAS is highlighted in blue. Corresponding adenines at off-target sites are highlighted in red. **(F)** Editing efficiency by Sanger sequencing of target adenines at on-target ( $79.3 \pm 4.7\%$ ) and potential off-target sites ( $<1.0\%$ ) for hEx45g5 in  $\Delta$ Ex44 iPSCs. Data are mean  $\pm$  s.d.  $n = 3$  independent replicates.

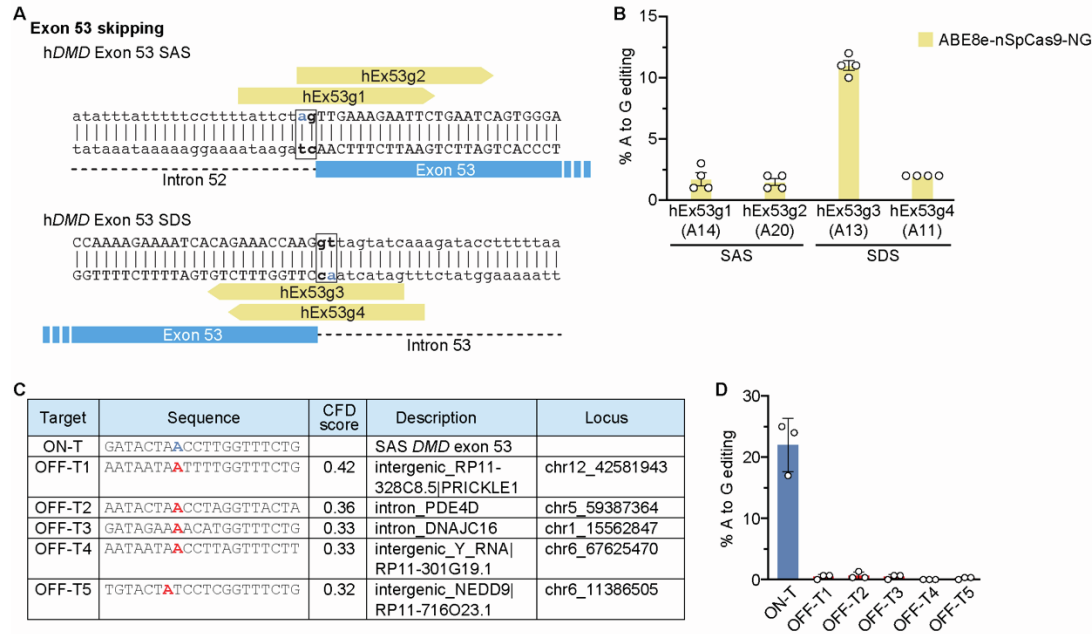


**Figure S3. Identification of the most efficient ‘single-swap’ guide for exon skipping of *DMD* exon 53.** (A) Schematic of candidate sgRNAs for single-swap editing at the SAS or SDS of *DMD* exon 53. Target adenines in relation to candidate sgRNAs are indicated in blue. Canonical splice site motifs are in bold. (B) Editing efficiency by Sanger sequencing of target adenine using candidates sgRNAs with ABE8e-nSpCas9-NG following transient transfection in HEK293T cells. The editing efficiency of the most efficient guide, hEx53g3, is  $11.0 \pm 0.8\%$ . (C) Candidate off-target sites within the human genome for hEx53g3 as identified by CRISPOR and ranked by CFD score. Target adenine of exon 53 SDS is highlighted in blue. Corresponding adenines at off-target sites are highlighted in red. (D) Editing efficiency by Sanger sequencing of target adenines at on-target ( $22.0 \pm 4.4\%$ ) and potential off-target sites ( $<0.7\%$ ) for hEx53g3 in  $\Delta$ Ex52 iPSCs. Data are mean  $\pm$  s.d.  $n = 3$  independent replicates.

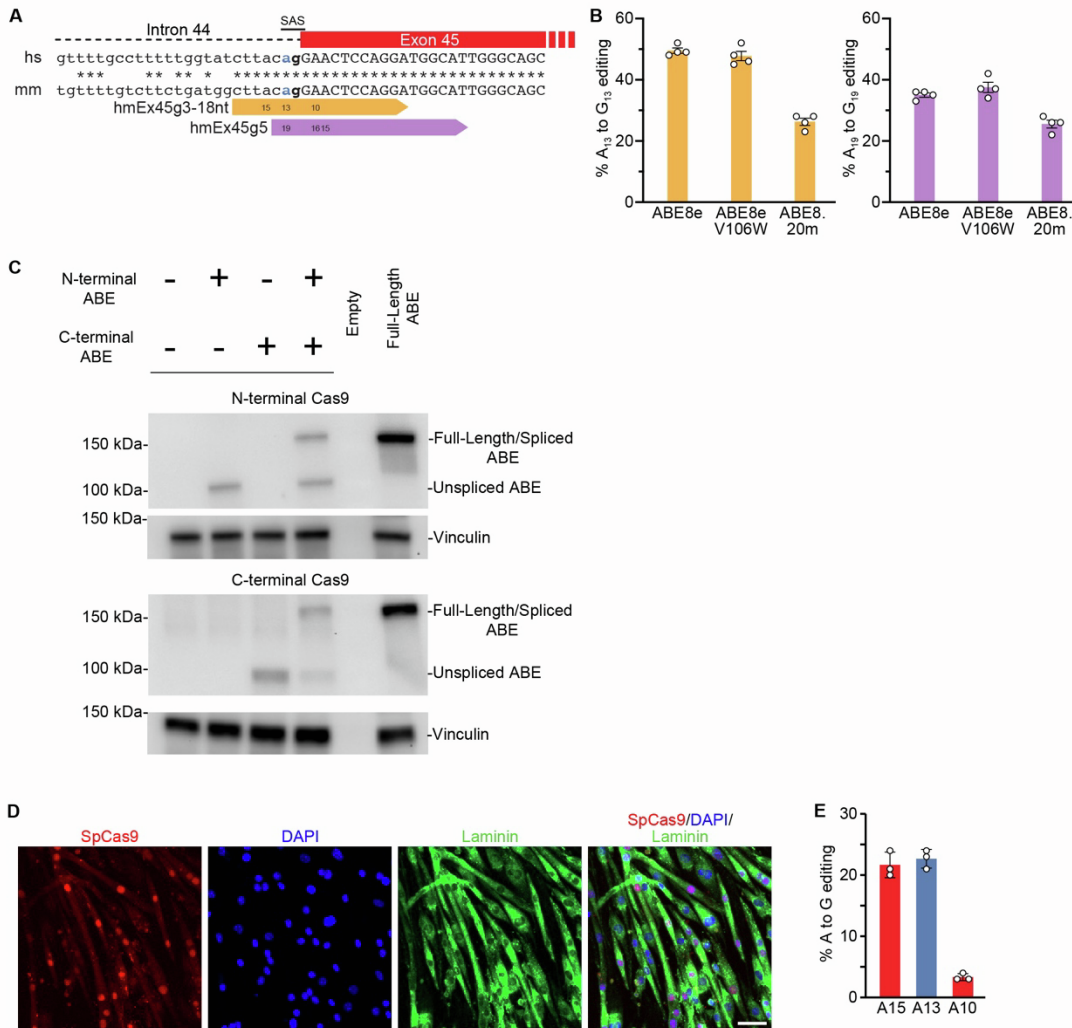


**Figure S4. Identification of the most efficient ‘single-swap’ guide for exon skipping of *Dmd* exon 45.** (A) Schematic of sgRNAs for single-swap editing at the SAS of *Dmd* exon 45 that can target both the human and mouse genome. Target adenines in relation to candidate sgRNAs are indicated in blue. Canonical splice site motifs are in bold. Homologous bases between the human (hs) and mouse (mm) genome are indicated by (\*). (B) Editing efficiency by Sanger sequencing of target adenine using candidate engineered deaminases and sgRNA hmEx45g3-18nt (left: 26.3 ± 2.4% to 49.5 ± 1.7%) or sgRNA hmEx45g5 (right: 25.5 ± 2.5% to 37.5 ± 3.3%). (C) Western blots using antibodies for N-terminal Cas9 or C-terminal Cas9 showing ABE8eV106W-nSpCas9

expression and splicing in HEK293T cells transiently transfected with plasmids encoding the N-terminal ABE, the C-terminal ABE, or the full-length ABE. Vinculin is the loading control. Expected molecular weights: N-terminal ABE, 105 kDa; C-terminal ABE, 100 kDa; full-length ABE, 186 kDa; vinculin, 124 kDa. **(D)** Transduction of C2C12 myotubes with the dual AAV ABE8e system results in robust ABE8eV106W-nSpCas9 protein expression and localization to the nucleus as shown by immunocytochemistry. ABE8eV106W-nSpCas9 protein is stained in red (antibody against N-terminal half of SpCas9), DAPI stains nuclei in blue, and laminin outlines myotubes in green. Scale bar, 25  $\mu$ m. **(E)** Editing efficiency by Sanger sequencing of editable adenines of genomic DNA from C2C12 myotubes infected with the dual AAV ABE8e system. Target adenine is colored in blue; editing efficiency is  $22.7 \pm 1.5\%$ . Data are mean  $\pm$  s.d.  $n = 3-4$  independent replicates.

**A**

| Target | Sequence  | CFD score | Description            | Locus          |
|--------|---|-----------|------------------------|----------------|
| ON-T   | **CTT <b>A</b> CAGGA <b>A</b> CTCCAGGA          |           | SAS <i>Dmd</i> exon 45 |                |
| OFF-T1 | AGCTT <b>A</b> CGG <b>A</b> ACTCAAGGT           | 0.39      | exon_Plxna3            | chrX_73375138  |
| OFF-T2 | GACTC <b>A</b> CGG <b>A</b> ACTCCAGGA           | 0.36      | exon_Col7a1            | chr9_108799469 |
| OFF-T3 | GGCC <b>A</b> AG <b>A</b> ACTCCAGAA             | 0.34      | intron_Col4a2          | chr8_11436024  |
| OFF-T4 | CACTT <b>A</b> TAG <b>A</b> AATCCAGGA           | 0.34      | exon_Lgals9            | chr11_78854104 |
| OFF-T5 | TTCTC <b>A</b> CG <b>A</b> A <b>A</b> ACTCCAGGA | 0.15      | intron_Ikzf3           | chr11_98406640 |

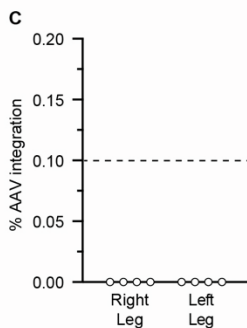
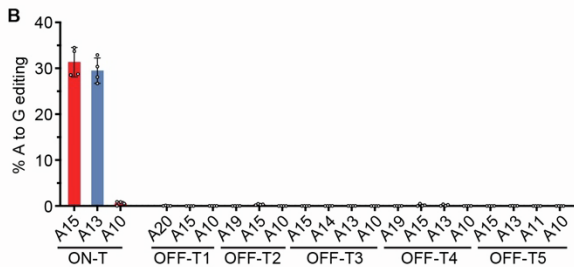


**Figure S5. Off-target editing for hmEx45g3-18nt in the mouse genome. (A)** Candidate off-target sites within the mouse genome for hmEx45g3-18nt as identified by CRISPOR. Target adenine of exon 45 SAS is highlighted in blue. Potential bystander adenines are highlighted in red. Editable adenines at off-target sites are highlighted in bold. **(B)** Editing efficiency by amplicon deep sequencing of editable adenines at on-target and potential off-target sites from the TA of mice treated with dual AAV ABE8e by IM injection. Target adenine is colored in blue; editing efficiency is  $29.5 \pm 2.7\%$ . Off-target editing is  $<0.3\%$  for all sites. **(C)** AAV integration frequency ( $<0.1\%$ ) at the on-target site from the TA of saline-treated right legs and dual AAV ABE8e-treated left legs of  $\Delta$ Ex44 mice. Data are mean  $\pm$  s.d.  $n = 4$  mice.



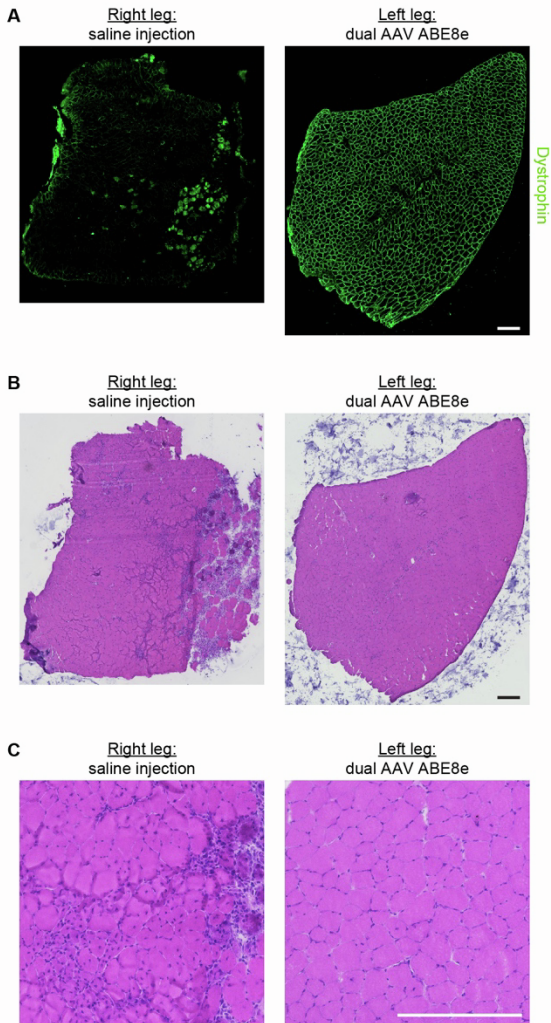


**Figure S6. Representative immunohistochemistry and histological staining from a  $\Delta$ Ex44 mouse treated with saline and dual AAV ABE8e. (A)** Immunohistochemistry for dystrophin of TA muscles from the saline-treated right leg and dual AAV ABE8e-treated left leg of a  $\Delta$ Ex44 mouse. Scale bar, 100  $\mu$ m. Dystrophin is stained in green. **(B)** H&E staining of TA muscles from the saline-treated right leg and dual AAV ABE8e-treated left leg of a  $\Delta$ Ex44 mouse at 4x magnification and **(C)** 20x magnification. Scale bar, 100  $\mu$ m.

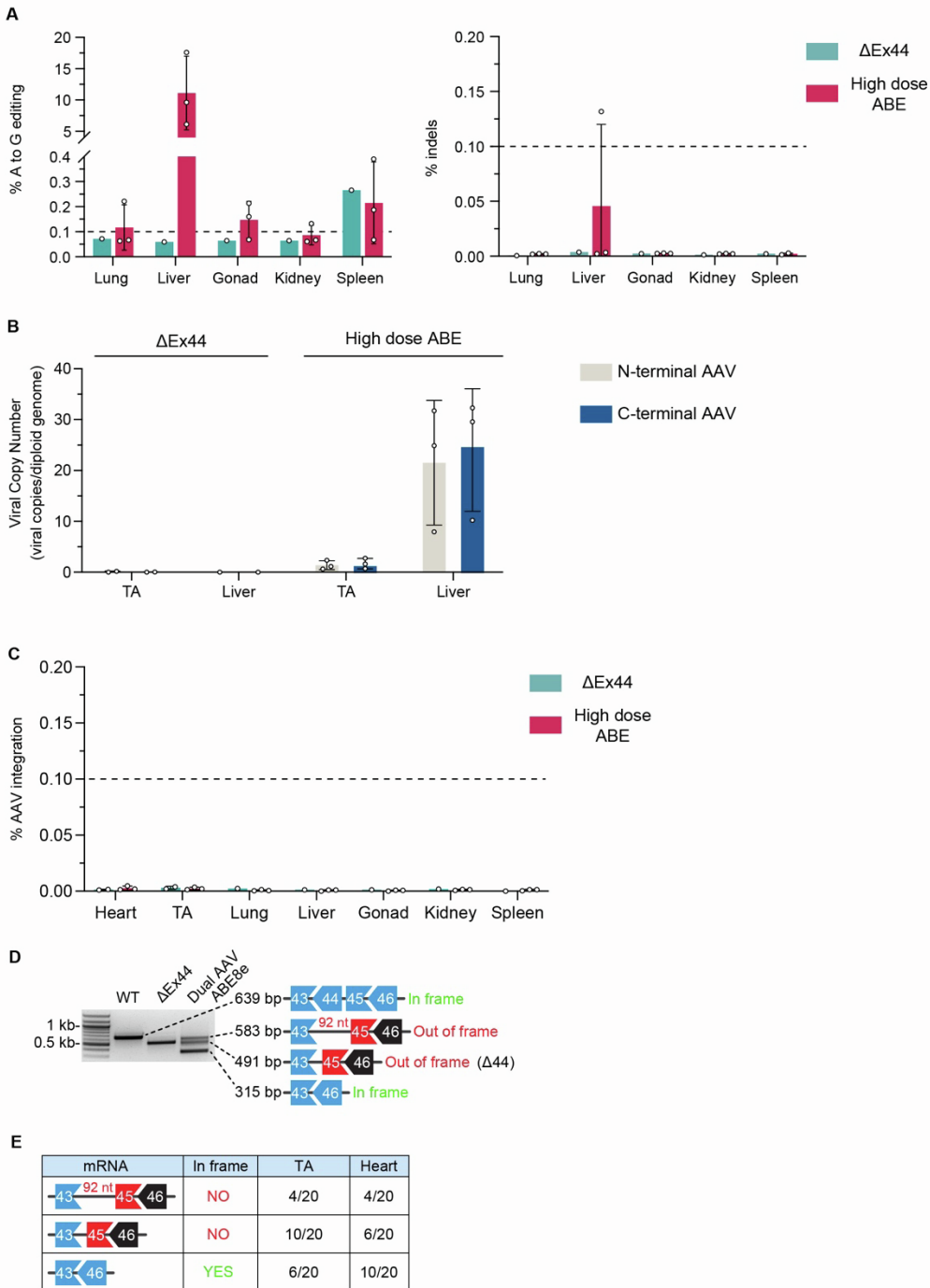


**Figure S7. Editing analysis in  $\Delta$ Ex44 mice treated by systemic injection of dual AAV ABE8e.** (A) Amplicon deep sequencing of DNA editing and indel frequency in lung, liver, gonad, kidney, and spleen tissue from high dose dual AAV ABE8e-treated and saline-treated  $\Delta$ Ex44 mice. Editing in the liver is  $11.1 \pm 5.9\%$ , and  $<0.2\%$  for all other tissues. Indel frequency

is <0.1% in all tissues. **(B)** Viral copy number of the N-terminal and C-terminal AAV halves from the liver ( $21.5 \pm 12.3$  N-terminal;  $24.0 \pm 12.0$  C-terminal) and TA ( $1.4 \pm 0.9$  N-terminal;  $1.7 \pm 1.0$  C-terminal) of high dose dual AAV ABE8e-treated and saline-treated  $\Delta$ ex44 mice, normalized to the diploid genome. **(C)** AAV integration frequency (<0.1%) at the on-target site in heart, TA, lung, liver, gonad, kidney, and spleen tissue of high dose dual AAV ABE8e-treated and saline-treated  $\Delta$ Ex44 mice. **(D)** RT-PCR analysis of mRNA from the heart of a WT mouse, a  $\Delta$ Ex44 mouse, and a  $\Delta$ Ex44 mouse treated with dual AAV ABE8e run. The cDNA of the WT is 639 bp; of the  $\Delta$ Ex44 is 491 bp; of the  $\Delta$ Ex44 with the intronic inclusion is 583 bp; of the  $\Delta$ Ex44 with exon skipping of exon 45 is 315 bp. **(E)** Frequency of transcript splicing events from the TA and heart of a  $\Delta$ Ex44 mouse treated with dual AAV ABE8e by TOPO-TA analysis.  $n=1-3$  mice.

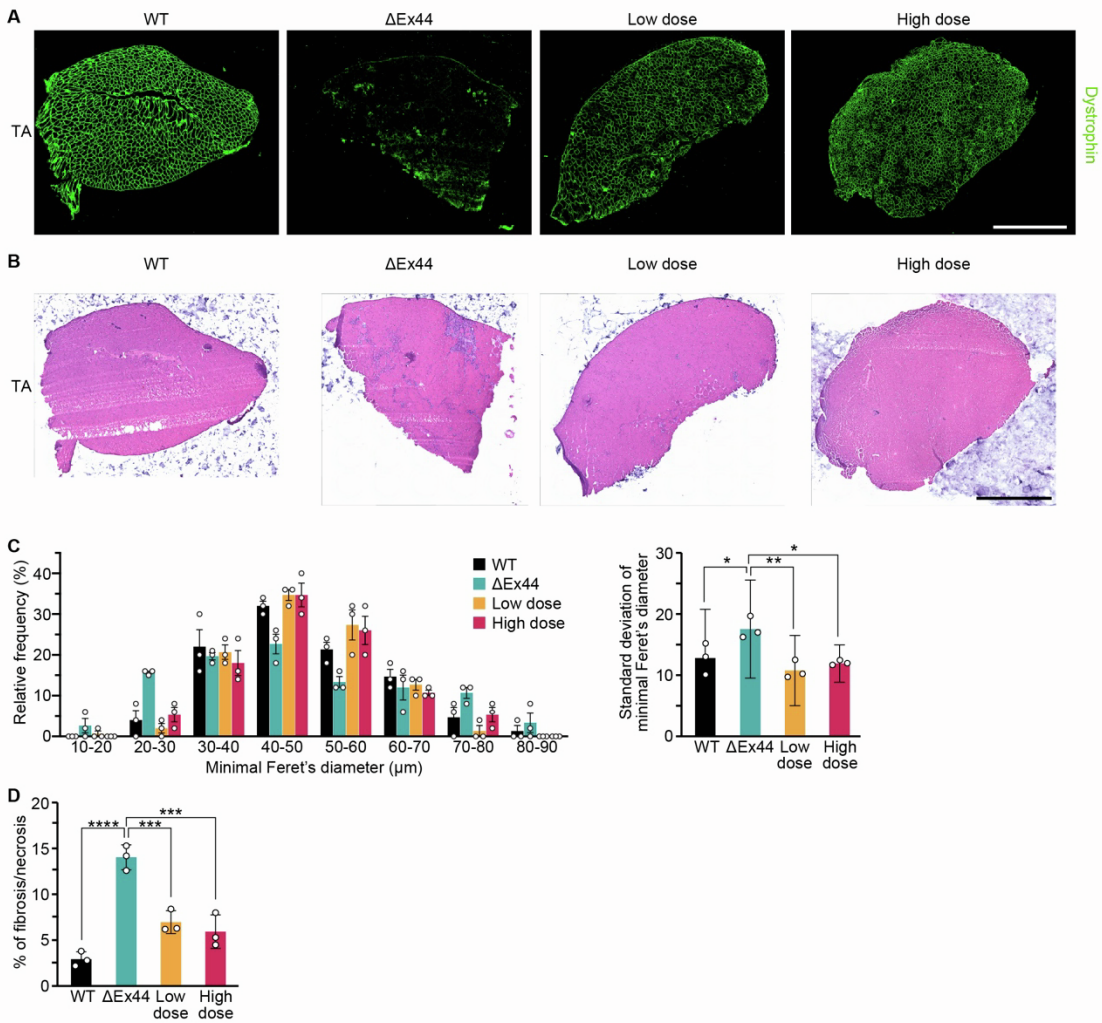


**Figure S8. Representative immunohistochemistry and histological staining from  $\Delta$ Ex44 mice treated with dual AAV ABE8e.** (A) Immunohistochemistry for dystrophin and (B) H&E staining of the TA of a WT mouse, a  $\Delta$ Ex44 mouse, and a  $\Delta$ Ex44 mouse treated with dual AAV ABE8e at the low and high doses. Scale bar, 1000  $\mu$ m. Dystrophin is stained in green. (C) Histogram of minimal Feret's diameter of myofibers and standard deviations, (Data are mean  $\pm$  s.e.m.) (WT, 12.8  $\pm$  8.0  $\mu$ m;  $\Delta$ Ex44, 17.5  $\pm$  8  $\mu$ m;  $\Delta$ Ex44 low dose, 10.8  $\pm$  5.7  $\mu$ m;  $\Delta$ Ex44 high dose, 11.9  $\pm$  3.0  $\mu$ m) and (D) percent area fibrosis or necrosis of TA muscles of a WT mouse (2.9  $\pm$  0.8%), a  $\Delta$ Ex44 mouse (14.0  $\pm$  1.4%), and a  $\Delta$ Ex44 mouse treated with dual AAV ABE8e at

the low ( $7.0 \pm 1.2\%$ ) and high ( $5.9 \pm 1.8\%$ ) doses.  $n = 3$  mice. Data are mean  $\pm$  s.d.  $*p < 0.05$ ,  $**p < 0.01$ ,  $***p < 0.001$ ,  $****p < 0.0001$  by ordinary one-way ANOVA.

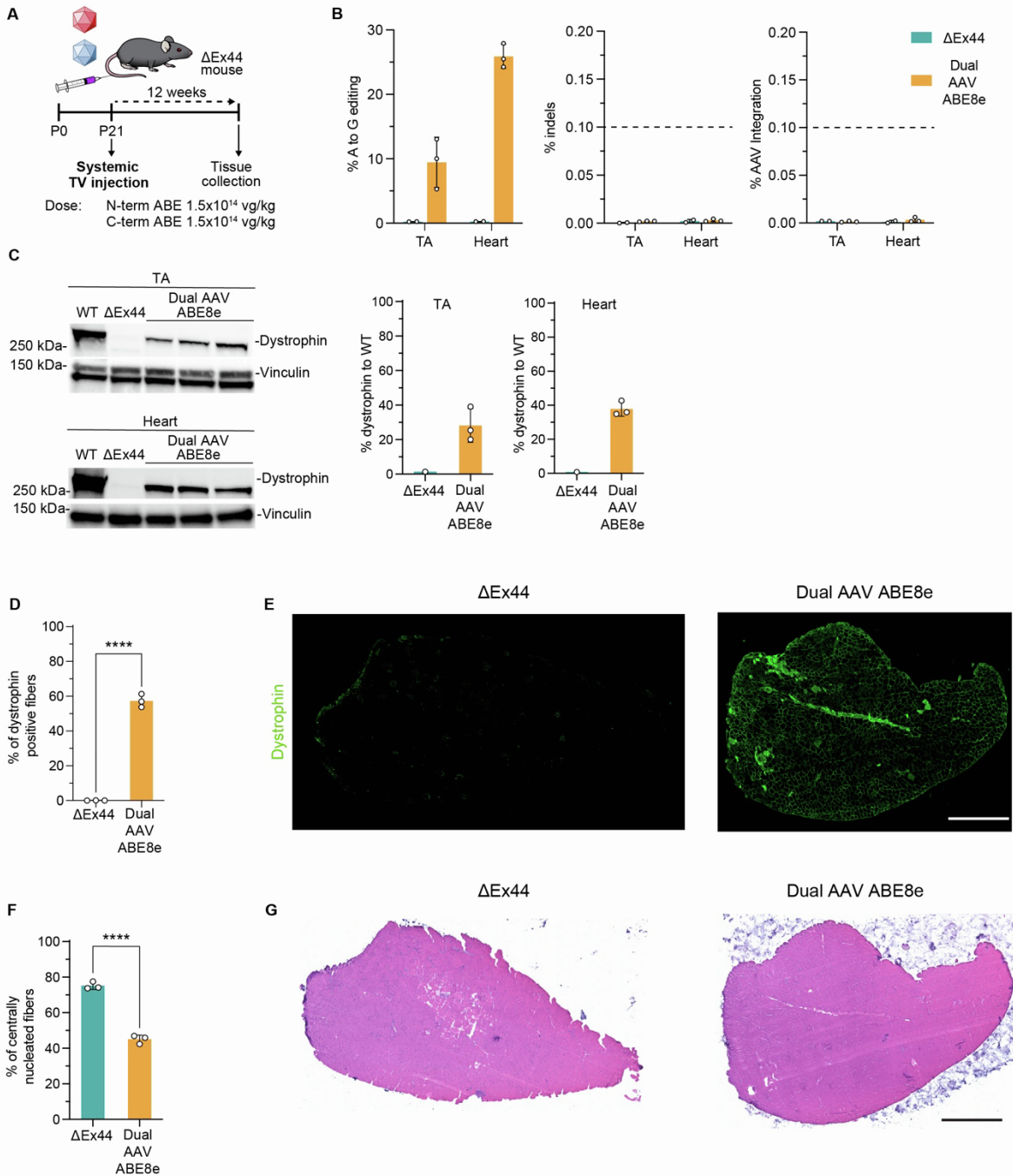


**Figure S9. Treatment of juvenile P21  $\Delta$ Ex44 mice with dual AAV ABE8e. (A)** DNA editing efficiency in the heart ( $29.0 \pm 1.7\%$ ) and TA ( $10.3 \pm 2.5\%$ ), indel frequency ( $<0.1\%$ ), and AAV integration frequency ( $<0.1\%$ ) by amplicon deep sequencing and **(B)** dystrophin protein expression in the heart ( $28.2 \pm 9.8\%$ ) and TA ( $37.8 \pm 4.3\%$ ) of P21  $\Delta$ Ex44 mice treated with dual

AAV ABE8e. Vinculin is the loading control. Relative intensity is measured as dystrophin expression normalized to vinculin compared to the WT. Western blots are quantified on the right panel. **(C)** The percentage of dystrophin positive fibers quantified from **(D)** immunohistochemistry sections of TAs from untreated ( $0.1 \pm 0.1\%$ ) and dual AAV ABE8e treated  $\Delta$ Ex44 mice ( $57.3 \pm 3.8\%$ ). Dystrophin is stained in green. **(E)** The percentage of centrally nucleated fibers from **(F)** H&E sections of TAs from untreated ( $75.2 \pm 2.1\%$ ) and dual AAV ABE8e treated  $\Delta$ Ex44 mice ( $45.1 \pm 2.4\%$ ). Scale bar, 1000  $\mu$ m. Data are mean  $\pm$  s.d.  $n = 1-3$  mice. \*\*\*\* $p < 0.0001$  by unpaired t-test.

**Table S1. Summary of oligos.** Please see attached Excel file for sequences.

**Table S2. Sequences of AAV constructs.** Please see attached Excel file for sequences.